Acta Cryst. (1976). A32, 883

X-ray Diffraction Study of Short-Range-Order Diffuse Scattering from Disordered Cu–29·8 at. % Pd Alloy

BY KEN-ICHI OHSHIMA* AND DENJIRO WATANABE
Department of Physics, Tohoku University, Sendai, Japan

AND JIMPEI HARADA
Department of Applied Physics, Nagoya University, Nagoya, Japan

(*Received* 23 *January* 1976; *accepted* 2 *April* 1976)

The diffuse X-ray scattering from a single crystal of disordered Cu–29·8 at.% Pd alloy was measured at room temperature. A fourfold splitting of the diffuse scattering due to short-range order was observed at the 110 reciprocal lattice point, in good agreement with the result previously obtained by electron diffraction. With the use of the method proposed by Borie & Sparks [*Acta Cryst.* (1971), A27, 198–201] the short-range-order parameters were determined by separating the other components of the diffuse scattering, *i.e.* size effect, Huang and thermal diffuse scattering, from the observed intensity data. It was revealed from this analysis that the order parameters beyond the 15th neighbour shell play an important role in characterizing this short-range-order diffuse scattering, although their magnitudes are small compared with those of the lower order parameters. Based on the ordering theory valid above the critical temperature the atomic-pair-interaction potential ratios were also obtained. It is shown that the pair-interaction potential is of long range and oscillates with distance. A comparison is made between the present result and the form of long-range oscillatory potential predicted by the conduction-electron screening model, and then the form of the Fermi surface is discussed.

I. Introduction

The short-range-order diffuse scattering from disordered Cu–Pd alloys has been studied by means of electron diffraction methods by Ohshima & Watanabe (1973). Characteristic fourfold splitting of diffuse scattering was observed at 100, 110 and equivalent positions in reciprocal space in the composition range from about 13 to 60 at.% Pd, and it was revealed that the split maxima correspond to the intersections of slightly curved diffuse streaks around the 100 and 110 positions and their separation increases with Pd content. The result was interpreted in terms of the Fermi surface imaging theory proposed by Krivoglaz (1969), and it was concluded that the pair-interaction potential in this alloy system originates mainly from conduction electrons and the diffuse scattering reflects the flat sections of the Fermi surface. A similar interpretation has also been given to the diffuse scattering observed from other disordered alloys, *e.g.* Cu–Au system (Moss, 1969), Cu_3Au with additional element of Pd or In (Hashimoto & Ogawa, 1970), Cu-rich Cu–Al alloys (Scattergood, Moss & Bever, 1970), Cu–Pt system (Oshima & Watanabe, 1973) and Au–Pd system (Ohshima & Watanabe, 1976).

If the intensities of short-range-order diffuse scattering are measured quantitatively, the magnitude and sign of the short-range-order parameters (or pair-correlation functions) can be obtained, and then the nature of the pair-interaction potentials can be acquired (Cowley, 1950; Clapp & Moss, 1966). Quantitative X-ray intensity measurements of the short-range-order diffuse scattering have, therefore, been performed on many binary alloys since 1950. However, the short-range-order parameters which actually reflect such characteristic features of diffuse scattering as mentioned above have not been obtained yet from X-ray measurements, mainly because of the lack of angular resolution involved in the X-ray diffractometer for the measurement of weak diffuse intensity as pointed out by Watanabe & Fisher (1965). It is thus of great interest to observe the fine structure of the short-range-order diffuse scattering by the X-ray method with better resolution.

In the present paper, we report the results of X-ray measurements obtained, from a disordered Cu–29·8 at.% Pd alloy quenched from 500°C, by improving the resolution of an X-ray diffractometer. The Cu–29·8 at.% Pd alloy forms a solid solution with a face-centred cubic structure above the ordering temperature $T_c \simeq 330$°C (Schubert, Kiefer, Wilkens & Haufler, 1955). Below T_c, this alloy has a two-dimensional antiphase domain structure, where the fundamental cell consists of a face-centred tetragonal atomic arrangement of the $L1_2$ type (Watanabe & Ogawa, 1956; Hirabayashi & Ogawa, 1957). This composition of the alloy was chosen in the present study, because T_c is rather low and the quenched specimen retains the short-range-ordered state existing at temperatures above T_c, as already confirmed by electron diffraction experiments (Ohshima & Watanabe, 1973).

* Present address: Department of Applied Physics, Nagoya University, Nagoya, Japan.

It is shown that the fourfold splitting of the short-range-order diffuse scattering at 110 reciprocal lattice point can be observed very clearly. The short-range-order parameters and also the ratios of pair-interaction potentials are then determined by analysing the intensity data on the basis of the method proposed by Borie & Sparks (1971). A comparison is made between the result for the pair-interaction and the form of the long-range interaction attributed to the conduction-electron screening of the ions.

II. Procedures of experiment and analysis

An alloy single crystal was grown in a high-purity alumina crucible, by the Bridgman technique. The materials used were 99·999% Cu and 99·9% Pd. The ingot was homogenized by vacuum annealing at 1000 °C for 5 d. A sample slice of 11 mm in diameter and 1·5 mm thick was cut parallel to a (210) plane from this ingot. The slice was polished mechanically and etched chemically in ferric chloride solution to remove the distorted surface layer. The crystallographic orientation was then examined and it was found that the surface normal deviates from [210] towards [100] by 5·5°. The specimen was annealed at 500°C for 13 d in a vacuum and then quenched in ice brine. The surface was again etched chemically to remove the oxide layer. The measured lattice parameter of the quenched specimen was $3{\cdot}710 \pm 0{\cdot}001$ Å. This value corresponds to the composition $29{\cdot}8 \pm 0{\cdot}4$ at.% Pd, according to the lattice parameter *vs* composition relation given in the literature (Pearson, 1958).

The X-ray intensity measurements were made by using a Rigaku four-circle goniometer attached to a rota-unit of an X-ray generator (Rigaku Rotaflex). This X-ray diffractometer unit was specially designed for the purpose of the intensity measurement of the weak diffuse scattering such as shown in the present study. The incident beam, Cu $K\alpha$ radiation, from a Cu target was monochromated by a doubly bent LiF crystal and it focused at the receiving slit vertically and at the specimen position horizontally. The horizontal and vertical divergences of the beam were 0·9 and 1·2°, respectively. The size of the receiving slit was adjusted in such a way that the resolution in reciprocal space corresponds to $0{\cdot}014 \times 0{\cdot}010 \times 0{\cdot}022$ Å^{-3} at $2\theta = 60°$. In order to eliminate both the $\lambda/2$ component from the monochromator and the fluorescent radiation from the sample, balanced Ni–Co filters placed before the sample were used in conjunction with a scintillation counter and a pulse-height analyser. The stability of the X-ray source was monitored by measuring the back scattering from an Al foil put on the slit between the monochromator and the sample. Reproducibility of the intensities at equivalent positions in reciprocal space was better than 5%. The data were obtained at room temperature (20°C).

The measured intensities were converted to absolute units (electron units per atom) by comparing them with the intensity scattered from polystyrene (C_8H_8) at $2\theta = 100°$ (Sparks & Borie, 1966). A 5% correction for multiple scattering from C_8H_8 was applied (Warren & Mozzi, 1966; Strong & Kaplow, 1967). The intensity measurement from C_8H_8 enables us to determine also the power of the incident beam. In the present experiment it was estimated as $(3{\cdot}97 \pm 0{\cdot}12) \times 10^8$ photons s^{-1}. It should be noticed that this value is more than seven times as large as that of the diffuse scattering measurements found so far in the literature, and the resolution of the present measurement is much better. For example, the power was $5{\cdot}44 \times 10^7$ photon s^{-1} in the experiments recently performed by Gragg & Cohen (1971) and Ericsson & Cohen (1971).

Background and scattering by air were estimated by using a lead beam trap in place of the sample, and the correction subtracted from the measured intensity. Contribution from Compton scattering was also eliminated from the intensity data after conversion to absolute units with the Bewilogua formula. The dispersion correction for the atomic scattering factors and the skew correction for absorption (Wooster, 1962) were also applied to the data. The diffuse intensity in regions of Bragg peak overlap was obtained by smooth extrapolation of the intensity in regions far away from the Bragg peaks.

The resulting diffuse intensity I_D consists of contributions from both the short-range-order diffuse scattering and the modulations resulting from static and thermal displacements of atoms from lattice points. The contribution of short-range order has to be separated from the total intensity distribution. When up to quadratic terms in the atomic displacements are included, I_D can be written as the sum of three terms:

$$I_D = N x_A x_B (f_A - f_B)^2 [I(\mathrm{SRO}) + I(\mathrm{SE}) + I(\mathrm{TDS+H})] \,. \quad (1)$$

where I(SRO) is the scattering due to short-range order, I(SE) the size-effect modulation term and I(TDS + H) the contributions from thermal diffuse scattering and Huang scattering. N is the number of atoms irradiated, x_A and x_B the atom fractions of components A and B, respectively, and f_A and f_B their atomic scattering factors. Each term in equation (1) is written as a series:

$$I(\mathrm{SRO}) = \sum_l \sum_m \sum_n \alpha_{lmn} \cos \pi l h_1 \cos \pi m h_2 \cos \pi n h_3 \,, \quad (2)$$

$$\begin{aligned} I(\mathrm{SE}) = -\sum_l \sum_m \sum_n \big(& h_1 \gamma^x_{lmn} \sin \pi l h_1 \cos \pi m h_2 \cos \pi n h_3 \\ & + h_2 \gamma^y_{lmn} \cos \pi l h_1 \sin \pi m h_2 \cos \pi n h_3 \\ & + h_3 \gamma^z_{lmn} \cos \pi l h_1 \cos \pi m h_2 \sin \pi n h_3 \big) \,, \end{aligned} \quad (3)$$

$$\begin{aligned} I(\mathrm{TDS+H}) = \sum_l \sum_m \sum_n \big[& (h_1^2 \delta^x_{lmn} + h_2^2 \delta^y_{lmn} + h_3^2 \delta^z_{lmn}) \\ & \times \cos \pi l h_1 \cos \pi m h_2 \cos \pi n h_3 \\ & + h_1 h_2 \varepsilon^{xy}_{lmn} \sin \pi l h_1 \sin \pi m h_2 \cos \pi n h_3 \\ & + h_2 h_3 \varepsilon^{yz}_{lmn} \cos \pi l h_1 \sin \pi m h_2 \sin \pi n h_3 \\ & + h_3 h_1 \varepsilon^{zx}_{lmn} \sin \pi l h_1 \cos \pi m h_2 \sin \pi n h_3 \big] \,. \end{aligned} \quad (4)$$

The integers l,m,n define a particular lattice site according to the relation

$$\mathbf{r}_{lmn}=l\frac{\mathbf{a}_1}{2}+m\frac{\mathbf{a}_2}{2}+n\frac{\mathbf{a}_3}{2},$$

where $\mathbf{a}_1$, $\mathbf{a}_2$ and $\mathbf{a}_3$ are the translation vectors of the cubic unit cell, and h_1, h_2 and h_3 are the continuous coordinates in reciprocal space and equal to the usual Miller indices at the reciprocal lattice points. The α_{lmn} are the short-range-order parameters defined by

$$\alpha_{lmn}=1-\frac{P^{AB}_{lmn}}{x_B}, \tag{5}$$

where P^{AB}_{lmn} is the probability of finding a **B** atom at the end of a vector $\mathbf{r}_{lmn}$ when the origin is occupied by an A atom. Other Fourier coefficients are given by

$$\gamma^x_{lmn}=2\pi[F_{AA}\langle x^{AA}_{lmn}\rangle+F_{AB}\langle x^{AB}_{lmn}\rangle+F_{BB}\langle x^{BB}_{lmn}\rangle], \tag{6}$$

$$\delta^x_{lmn}=-2\pi^2[F_{AA}\langle(x^{AA}_{lmn})^2\rangle+F_{AB}\langle(x^{AB}_{lmn})^2\rangle+F_{BB}\langle(x^{BB}_{lmn})^2\rangle], \tag{7}$$

$$\varepsilon^{xy}_{lmn}=-4\pi^2[F_{AA}\langle(x^{AA}_{lmn}y^{AA}_{lmn})\rangle+F_{AB}\langle(x^{AB}_{lmn}y^{AB}_{lmn})\rangle+F_{BB}\langle x^{BB}_{lmn}y^{BB}_{lmn})\rangle], \tag{8}$$

where

$$F_{AA}=\frac{f_A^2}{(f_A-f_B)^2}\left(\frac{x_A}{x_B}+\alpha_{lmn}\right), \tag{9}$$

$$F_{AB}=\frac{2f_Af_B}{(f_A-f_B)^2}(1-\alpha_{lmn}), \tag{10}$$

$$F_{BB}=\frac{f_B^2}{(f_A-f_B)^2}\left(\frac{x_B}{x_A}+\alpha_{lmn}\right). \tag{11}$$

The coefficients γ^y_{lmn}, γ^z_{lmn}, δ^y_{lmn}, δ^z_{lmn}, ε^{yz}_{lmn} and ε^{zx}_{lmn} are expressed similarly. The quantity $\langle x^{\mu\nu}_{lmn}\rangle$ denotes the average displacement along the [100] axis between μ–ν atom pairs separated by the vector $\mathbf{r}_{lmn}$, with similar definitions for the quantities $\langle(x^{\mu\nu}_{lmn})^2\rangle$ and $\langle x^{\mu\nu}_{lmn}y^{\mu\nu}_{lmn}\rangle$.

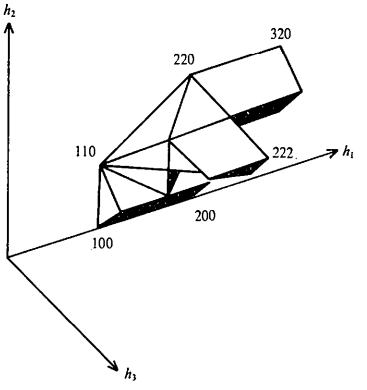

Fig. 1. The volume in reciprocal space, over which intensity measurements were made.

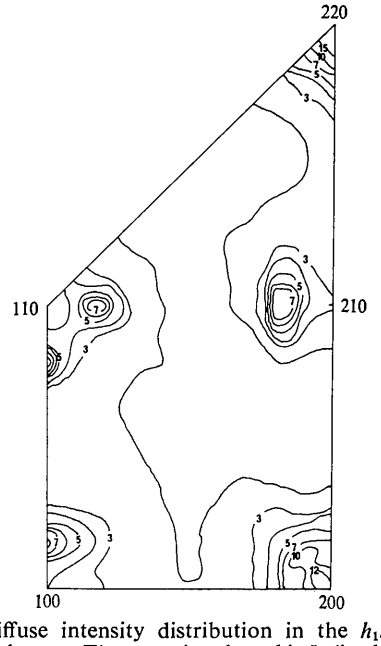

Fig. 2. Diffuse intensity distribution in the h_1h_20 plane of reciprocal space. The quantity plotted is I_D (in electron units)/$Nx_Ax_B(f_A-f_B)^2$.

In the present study, the diffuse intensity was measured at each of 2763 points in reciprocal space over the volume shown in Fig. 1, and the method developed by Borie & Sparks (1971) was employed to separate the observed intensity into various components. This method of analysis is, however, based on an assumption that $f_A/(f_A-f_B)$ and $f_B/(f_A-f_B)$ do not change as rapidly as a function of $\sin\theta/\lambda$ within the volume measured in reciprocal space. In the present case such an assumption is confirmed to be valid within 8%. The volume chosen for the measurement (Fig. 1) was scanned at the interval of $\Delta h_i=\frac{1}{40}$, in terms of the distance between the 000 and 200 fundamental spots, in the regions where the diffuse maxima have been observed and at the interval of $\Delta h_i=\frac{1}{20}$ in the other regions. An interpolation of the data was made in the latter regions to estimate the intensities at the interval of $\Delta h_i=\frac{1}{40}$. The intensities of 9154 positions in the volume were then used in the analysis.

III. Results and interpretation

III.1. *Determination of the short-range-order parameters* α_{lmn}

Fig. 2 shows the diffuse X-ray intensity distribution observed on the (h_1h_20) reciprocal lattice plane, where the contributions from the Compton scattering have been subtracted with the use of theoretical calculation and those from the Bragg scattering near the fundamental spots by an extrapolation method. The intensities in Fig. 2 are expressed in Laue monotonic units.

Intensity distribution due to short-range-order diffuse scattering only was separated from the total intensity by using the method of Borie & Sparks. The result on the (h_1h_20) reciprocal plane is shown in Fig. 3. At the 110 position, a fourfold splitting of diffuse scattering and the slightly curved diffuse streaks connect-

ing these four split maxima can be clearly seen. Besides, the intensities of the diffuse maxima are noticed to be approximately twice as much as those of the diffuse streaks. From this fact the conclusion given previously from the electron diffraction experiment (Ohshima & Watanabe, 1973) is confirmed quantitatively, that the diffuse split maxima correspond simply to the intersections of the diffuse streaks.

The separation between the diffuse maxima relative to the distance between the two fundamental spots, 000 and 200, which was denoted by m in the previous paper, was found to be $0{\cdot}13 \pm 0{\cdot}01$ in the present measurement. This value is in good agreement with that obtained by electron diffraction within the experimental error.

By performing the Fourier inversion of the intensity, short-range-order parameters α_{lmn} were determined up to the 47th shell. The results are given in Table 1. It is noticed from the table that the value of 1·786 obtained for α_{000} is quite large though it should be unity theoretically. This amount of disagreement, however, is common in most of the absolute measurements of the X-ray diffuse scattering as seen in the literature.

It is interesting to compare the sign and magnitude of α_{lmn} obtained for this alloy with those for a Cu_3Au type ordered structure (α'_{lmn}). The values of α_{lmn} are plotted against r_{lmn} in Fig. 4, where they are classified into two groups; all the indices l, m and n are even in the first group and only one of them is even in the second group. For the stoichiometric Cu_3Au-type ordered structure, the value of α'_{lmn} is independent of r_{lmn} and unity for the first group and $-\frac{1}{3}$ for the second. The α'_{lmn} parameters corresponding to the composition of the present alloy are estimated to be 0·77 and −0·26 for the two groups, provided that the excess Pd atoms are distributed statistically over the Cu atom sites in the ordered state. As seen in Table 1 and Fig. 4, the absolute magnitude of α_{lmn} decreases with an increase in distance from the origin, $(l^2+m^2+n^2)^{1/2}$, as a general tendency. However, it is noticed that some of the α_{lmn} parameters change sign from plus to minus for the first group and *vice versa* for the second group, beyond the eighth-neighbour shell.

Table 1. *Experimental values of short-range-order parameters,* α_{lmn} ($\times 10^3$)

i	lmn	α_{lmn}	i	lmn	α_{lmn}
	000	1786	28	730	−2
1	110	−105	29	732	−2
2	200	178		651	8
3	211	−28	30	800	−3
4	220	76		811	5
5	310	−39	31	741	2
6	222	46		554	1
7	321	−7	32	820	2
8	400	40		644	−8
9	330	−16	33	653	6
	411	13	34	822	1
10	420	9		660	−4
11	332	−7		831	−1
12	422	0	35	750	−5
13	510	−16		743	2
	431	8	36	662	−4
14	521	−2	37	752	−3
15	440	−7	38	840	1
16	530	−7	39	910	−7
	433	6		833	2
17	600	1	40	842	−1
	442	−6		921	1
18	611	12	41	761	3
	532	−6		655	3
19	620	2	42	664	−8
20	541	7		930	−2
21	622	−2	43	851	3
22	631	6		754	1
23	444	−8	44	932	−3
	710	−9		763	4
24	550	−11	45	844	−3
	543	4		941	1
25	640	−6	46	853	2
	721	1		770	−2
26	633	6	47	860	−2
	552	−7		1000	4
27	642	−6			

To investigate how the characteristic fine structure of short-range-order diffuse scattering observed in this alloy is reflected in the value of α_{lmn}, the diffuse intensity map was synthesized using the α_{lmn} given in Table 1. Fig. 5(*a*) and (*b*) shows two examples of the intensity maps synthesized: the parameters up to the 15th neighbour were used in (*a*), and in addition those of more distant neighbours of absolute values larger than 0·005 were also included in (*b*). In both cases, the value of α_{000} was assumed to be unity. As expected from the usual theory of Fourier inversion it is seen that fairly high order parameters, such as those beyond the 15th neighbour shell, are needed to reproduce the characteristic fine structure of the measured diffuse scattering; *i.e.* their signs and magnitudes play an important role in causing the appearance of diffuse streaks

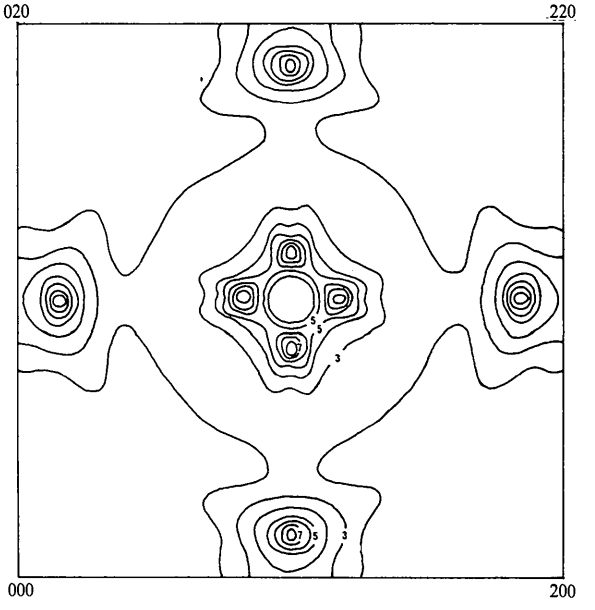

Fig. 3. The short-range-order component of diffuse scattering I(SRO) in the h_1h_20 plane.

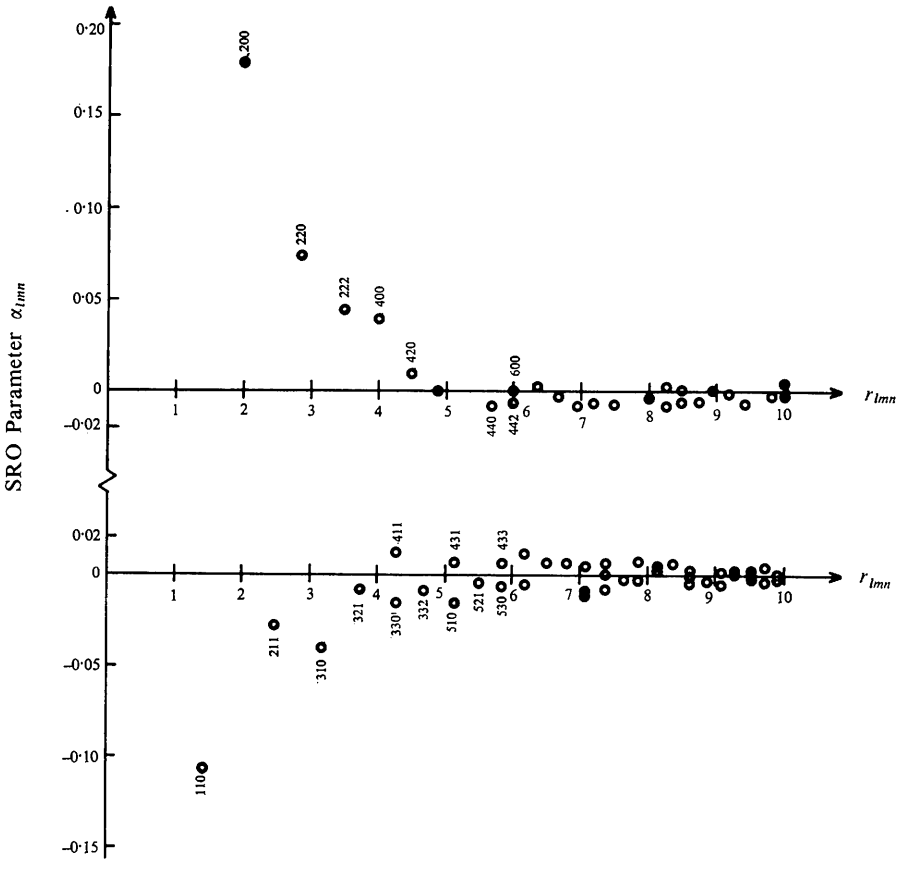

Fig. 4. Short-range-order parameters α_{lmn} *vs* $r_{lmn}=(l^2+m^2+n^2)^{1/2}$. The parameters are classified into two groups: all the indices l, m and n are even in the upper plot and only one of them is even in the lower plot.

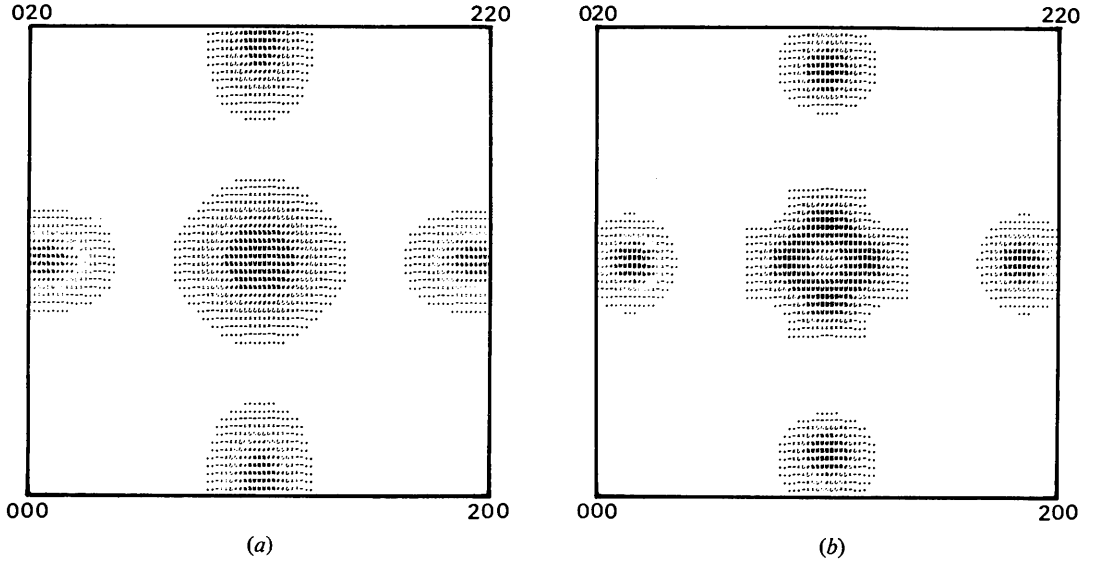

Fig. 5. Diffuse scattering intensity synthesized from experimental α_{lmn} parameters. The parameters up to 15th neighbour were used in (*a*), and in addition those of more distant neighbours of absolute values larger than 0·005 were also included in (*b*). The α_{000} value was assumed to be unity in both cases.

and split diffuse mixima, even though their absolute values are small compared with those of the lower order parameters.

III.2. *Interpretation of atomic displacement parameters*

Fig. 6 (*a*) and (*b*) shows the intensity distribution of the diffuse scattering due to size effect I(SE) and the intensity distribution from thermal diffuse and Huang scattering I(TDS + H), respectively. It is noticed that the intensity modulation due to the size effect concentrates at a position slightly off the Bragg peak (Fig. 6*a*). This is because the odd function of I(SE) is zero at the fundamental reflexion positions, as seen in equation (3). On the other hand, the I(TDS + H) component elongates along the $\langle\bar{1}10\rangle$ direction from the Bragg peak 200 (Fig. 6*b*).

The atomic displacement parameters γ^x_{lmn}, γ^y_{lmn} and γ^z_{lmn} were obtained by performing the Fourier transformation of I(SE). They are presented in Table 2. The values are small compared with those for other alloys, *e.g.* the Ni–50 at.% Pd alloy, where γ^x_{110} and γ^x_{200} are 0·240 and −0·326, respectively (Lin & Spruiell, 1971).

Table 2. *Experimental values of atomic displacement parameters,* γ^x_{lmn}, γ^y_{lmn} *and* γ^z_{lmn} ($\times 10^3$)

lmn	γ^x_{lmn}	γ^y_{lmn}	γ^z_{lmn}
000	0	0	0
110	60	60	0
200	−36	0	0
211	−31	37	37
220	30	30	0
310	22	−1	0
222	23	23	23
321	32	18	−2
400	34	0	0
411	−7	17	17
330	15	15	0
420	25	17	0
332	8	8	13
422	14	7	7
431	11	23	10
510	19	−2	0
521	28	7	0
440	16	16	0
530	10	5	0
433	6	8	8
600	43	0	0
442	10	7	7
611	5	12	12
532	9	7	8

With the assumption that the average interatomic distance must be maintained constant in order to conserve the average volume, the weighted average of the displacements for all AA, AB, BA and BB pairs is zero for any coordination shell, and hence it is possible to rewrite equation (6), in terms of $\langle x^{AA}_{lmn}\rangle$ and $\langle x^{BB}_{lmn}\rangle$, as

$$\gamma^x_{lmn} = \frac{2\pi}{f_A - f_B}\left[\left(\frac{x_A}{x_B} + \alpha_{lmn}\right) f_A \langle x^{AA}_{lmn}\rangle - \left(\frac{x_B}{x_A} + \alpha_{lmn}\right) f_B \langle x^{BB}_{lmn}\rangle\right] . \quad (12)$$

Although it is not known how to recover $\langle x^{AA}_{lmn}\rangle$ and $\langle x^{BB}_{lmn}\rangle$ separately, the first nearest-neighbour atomic displacement can be estimated roughly from the value of γ_{110}. If numerical values for the present alloy are substituted into equation (12), we have the relation

$$\langle x^{PdPd}_{110}\rangle - (4{\cdot}193 \mp 0{\cdot}133)\langle x^{CuCu}_{110}\rangle = (0{\cdot}012 \pm 0{\cdot}001) , \quad (13)$$

where the ratios of scattering factors $f_A/(f_A - f_B)$ and $f_B/(f_A - f_B)$ were assumed to be constant and the errors were estimated from their variation across the angular range 24–90° in 2θ. Since it is reasonable to expect that $\langle x^{CuCu}_{110}\rangle$ and $\langle x^{PdPd}_{110}\rangle$ are negative and positive, respectively, we have the following result:

$$0 > \langle x^{CuCu}_{110}\rangle > -0{\cdot}003$$
$$0 < \langle x^{PdPd}_{110}\rangle < \quad 0{\cdot}012 .$$

It is interesting to compare these results with the values obtained from a hard-sphere model in which the atoms in the alloy are assumed to retain their size of the pure state. On the basis of this model, the displacements are estimated to be $\langle x^{CuCu}_{110}\rangle = -0{\cdot}026$ and $\langle x^{PdPd}_{110}\rangle = 0{\cdot}049$. It is noticed that these values are considerably larger than the experimental values for the alloy.

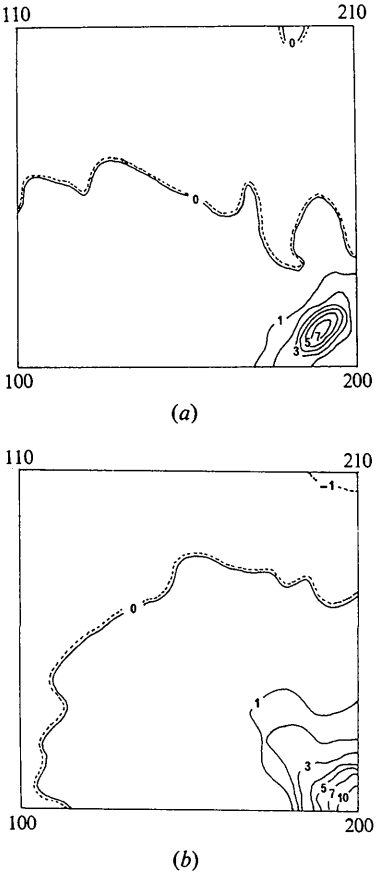

Fig. 6. Intensity distributions of atomic displacement modulations. (*a*) Size-effect modulation I(SE). (*b*) Thermal diffuse scattering and Huang scattering I(TDS + H).

The above estimation of the atomic displacements in the alloy is admittedly crude. It is, however, concluded from this comparison that the atoms in the alloy do not retain their proper sizes, the Cu atoms being enlarged and the Pd atoms compressed. This is consistent with the fact that the intensity asymmetry characteristic of the size-effect modulation is hardly observable in the diffuse split maxima at the 110 position in Fig. 2.

III.3. *Determination of the pair-interaction potential ratios*

In a linearized approximation for the correlation functions of a binary alloy, developed by Clapp & Moss (1966), the diffuse scattering intensity is expressed by

$$I(\mathbf{k}) = \frac{C}{1+2x_A x_B \beta V(\mathbf{k})}, \qquad (14)$$

where $V(\mathbf{k})$ is a Fourier transform of the pair-interaction potential, $V(\mathbf{r}) = \frac{1}{2}\{V^{AA}(\mathbf{r}) + V^{BB}(\mathbf{r}) - 2V^{AB}(\mathbf{r})\}$, between pairs of atoms separated by a vector $\mathbf{r}$. $\beta = 1/(k_B T)$ with k_B the Boltzmann constant and T the temperature. C is a normalization constant and is expressed

$$C = \left[\frac{1}{v_k}\int \frac{1}{1+2x_A x_B \beta V(\mathbf{k})}\,\mathrm{d}^3k\right]^{-1}, \qquad (15)$$

by the condition that the integral of $I(\mathbf{k})$ over a unit-cell volume of the reciprocal lattice, v_k, should be unity.

Using equation (14), the values of $V(\mathbf{k})$ can be obtained directly from the measured short-range-order diffuse scattering I(SRO), and then the pair-interaction potentials can be determined by Fourier inver-

Table 3. *Values of atomic-pair-interaction ratios* $V(r_{lmn})/V(r_{110})$ $(\times 10^3)$

$V(r_{110})$ is the pair-interaction potential between the first nearest-neighbour atoms and its sign is positive.

i	lmn	$V(r_{lmn})/V(r_{110})$	i	lmn	$V(r_{lmn})/V(r_{110})$
1	110	1000	28	730	−34
2	200	−1685	29	732	18
3	211	154		651	−29
4	220	−429	30	800	54
5	310	244	31	811	−50
6	222	−40		741	25
7	321	−50		554	1
8	400	−176	32	820	8
9	330	−21		644	32
	411	−66	33	653	−17
10	420	147	34	822	−4
11	332	−8		660	−12
12	422	97	35	831	45
13	510	43		750	−4
	431	−23		743	−10
14	521	−51	36	662	7
15	440	82	37	752	11
16	530	−36	38	840	−11
	433	0	39	910	57
17	600	2		833	−2
	442	−28	40	842	−15
18	611	−29	41	921	−37
	532	32		761	16
19	620	24		655	4
20	541	−21	42	664	13
21	622	−26	43	930	9
22	631	35		851	−27
23	444	−40		754	−9
24	710	36	44	932	22
	550	28		763	−11
	543	1	45	844	16
25	640	9	46	941	5
26	721	−33		853	−4
	633	−13		770	−3
	552	50	47	860	7
27	642	−24		1000	−2

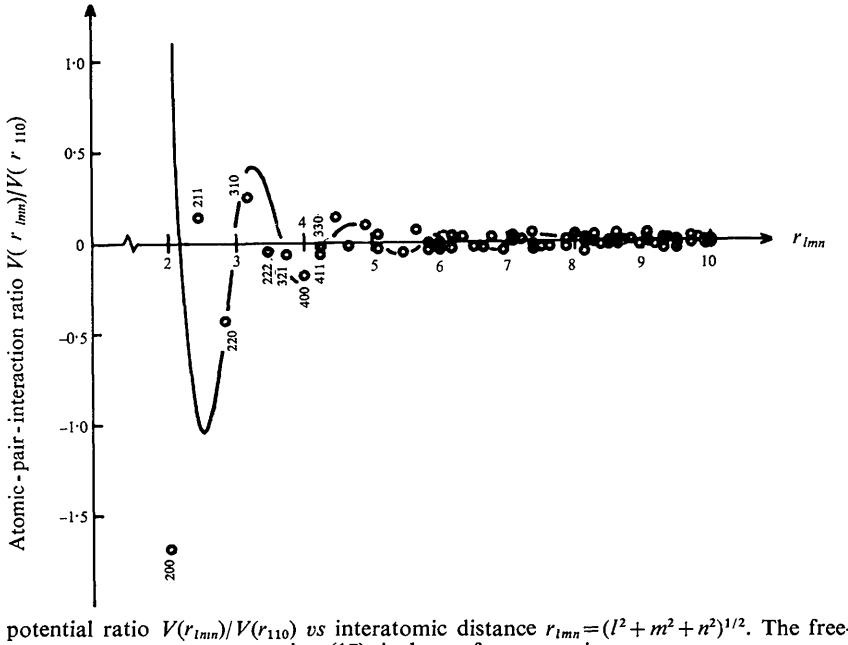

Fig. 7. Pair-interaction potential ratio $V(r_{lmn})/V(r_{110})$ *vs* interatomic distance $r_{lmn} = (l^2+m^2+n^2)^{1/2}$. The free-electron screening curve, equation (17), is drawn for comparison.

sion of $V(\mathbf{k})$. In applying equation (14) to the experimental data, however, a small error in the observed diffuse intensity $I^{obs}(\mathbf{k})$ away from the diffuse peak [*i.e.* near the fundamental reflexion where $I(\mathbf{k})$ is small] will be propagated by equation (14) as a large error in $V(\mathbf{k})$. Therefore, after taking the average $I^{obs}(\mathbf{k})$ away from the diffuse peak and smoothing out the fluctuation, the corresponding $V(\mathbf{k})$ values were obtained.

Performing the Fourier transformation of $V(\mathbf{k})$, the pair-interaction potential ratios $V(r_{lmn})/V(r_{110})$ were determined, where $V(r_{110})$ is the pair-interaction potential between the first nearest-neighbour atoms and has a positive value. The results are listed in Table 3 and plotted against the interatomic distance r_{lmn} in Fig. 7. It is evident from this plot that the pair-interaction potential is of long range and oscillates with distance.

In order to see the correlation between the characteristic fine structure of diffuse scattering and the pair-interaction potentials obtained, the diffuse intensity map was synthesized using the values given in Table 3, and it was demonstrated that the synthesized map gives diffuse maxima at the superlattice reflexion positions when only the first nine pair-interaction potentials are included, and that at least the first 18 potentials are needed to obtain the intensity map such as shown in Fig. 5(*b*).

It was thus confirmed that the long-range oscillatory pair-interaction potentials can reproduce very reliably the observed intensity distribution. They were then compared with the free-electron screening model for pair interactions between ions. According to Blandin & Deplanté (1963) and Harrison & Paskin (1963), the ratio of the pair-interaction potentials at large distances is given in the form

$$\frac{V(r_{lmn})}{V(r_{110})} = \frac{A\cos(2k_F a_0 r_{lmn}+\varphi)}{(r_{lmn})^3}, \qquad (16)$$

where k_F is the Fermi wave number and $2a_0$ is the unit-cell spacing. A is assumed to be a constant and φ is a phase factor. Since the quantity $2k_F a_0$ is related to the electron-per-atom ratio (e/a), it is rewritten as

$$\frac{V(r_{lmn})}{V(r_{110})} = \frac{A\cos[4{\cdot}911(e/a)^{1/3} r_{lmn}+\varphi]}{(r_{lmn})^3}. \qquad (17)$$

In the present case, the e/a value is calculated to be 0·702 from the composition, assuming the number of conduction electrons to be one for Cu and zero for Pd.

An attempt was made to fit equation (17) to the present results by adjusting the two parameters A and φ. However, it was not possible to find the screening curve which fits all the potential values. It is considered that this disagreement is ascribed to a non-spherical shape of the Fermi surface.

In fact, it is known that the shape of the Fermi surface of Cu–Pd alloys containing up to 60 at.% Pd bears some resemblance to that of Cu: the existence of flat sections of the Fermi surface normal to the ⟨110⟩ directions has been confirmed by an electron diffraction study (Ohshima & Watanabe, 1973), and the existence of the ⟨111⟩ necks by a positron annihilation study (Hasegawa, Suzuki & Hirabayashi, 1975).

Hence, the potentials along and close to both the directions ⟨110⟩ and ⟨111⟩ were neglected in the curve fitting, *i.e.* $V(r_{220})$, $V(r_{222})$, $V(r_{330})$, $V(r_{332})$ and $V(r_{440})$, and then comparison of the present result with equation (17) was made. The potentials, $V(r_{110})$ and $V(r_{200})$, were also discarded from the fitting, because the form of Friedel oscillation, equation (17), should be valid only at large distances. The solid curve in Fig. 7 is for the parameters $A=10{\cdot}0$ and $\varphi=1{\cdot}8$, and it appears to fit the experimental result.

For the flat portions of the Fermi surface, the interactions fall off in proportion to $(r_{lmn})^{-1}$, instead of $(r_{lmn})^{-3}$ (Roth, Zeiger & Kaplan, 1966), and the ratio of pair-interaction potentials along the ⟨110⟩ directions is given by

$$\frac{V(r_{l10})}{V(r_{110})} = \frac{A'\cos(2k'_F a_0 r_{l10}+\varphi')}{r_{l10}}. \qquad (18)$$

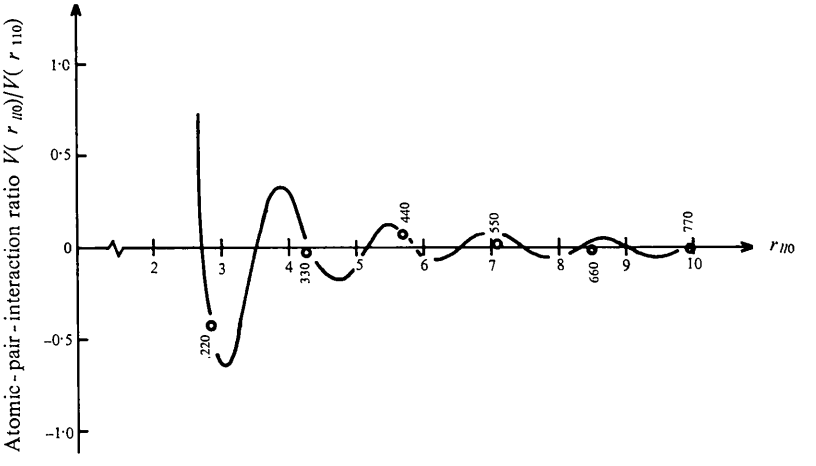

Fig. 8. The same plot as shown in Fig. 7 is compared with $(r_{l10})^{-1}$ curve, equation (18).

The potentials with indices *l*10 were compared with this equation, and a reasonable agreement was obtained between the observed values and the theoretical curve as shown in Fig. 8, where A' and φ' were chosen as 1·5 and 2·2, respectively. The Fermi wave number k'_F along the ⟨110⟩ direction is given by $k'_F = tk_F$, where t is the truncation factor representing the flatness of the Fermi surface and was estimated to be 0·917 for the present alloy composition from the result of the previous electron diffraction study. As seen from Fig. 8, the potential values of higher indices are very small and have a tendency to deviate from the curve, and it is suggested that the interactions along the ⟨110⟩ direction fall off slightly faster than $(r_{lmn})^{-1}$.

IV. Discussion and conclusion

In the present study, the short-range-order diffuse scattering with characteristic fourfold splitting was measured quantitatively by X-ray diffraction from a single crystal of a disordered Cu–29·8 at.% Pd alloy, and the short-range-order parameters α_{lmn}, atomic displacement parameters γ_{lmn}, and pair-interaction potential ratios $V(r_{lmn})/V(r_{110})$ were determined.

The result shows that the α_{lmn} parameters beyond the 15th neighbour shell play an important role in characterizing the intensity distribution of short-range-order diffuse scattering, although their absolute values are small compared with those of low order parameters. The pair-interaction potential is of long range and oscillatory, and at least the first 18 pair-interaction potentials are needed to reproduce the characteristic features of diffuse scattering. From the comparison of the pair-interaction potential ratios with the conduction-electron screening model, it has been revealed that the Fermi surface of the alloy has nearly flat regions in the ⟨110⟩ directions, and the conclusion of the previous electron diffraction study (Ohshima & Watanabe, 1973) has been confirmed. Except in the directions along and close to ⟨110⟩ and ⟨111⟩, the pair-interaction potentials are explained in terms of the spherical Fermi surface.

Several attempts have been made to determine the pair-interaction potentials from diffuse scattering data. Wilkins (1970) and Wilkins & Shirley (1975) have analysed the published data for disordered Cu_3Au, CuAu and Au–40 at.% Pd alloys, using the real-space formalism, and they have determined the first seven pair-interaction potential ratios $(V_2/V_1, V_3/V_1, \ldots)$ and have compared them with the free-electron screening model. They used the first 11 α_{lmn} parameters for Cu_3Au and the 14 parameters for CuAu and Au–40 at.% Pd alloys. As shown by the present analysis, however, the α_{lmn} parameters and the pair-interaction potentials at large distances influence the characteristic features of diffuse scattering, when the form of the Fermi surface is reflected in the distribution of diffuse scattering. In fact, the diffuse intensities with split maxima have been observed for Cu_3Au and CuAu alloys on the electron diffraction patterns (Raether, 1952; Sato, Watanabe & Ogawa, 1962; Marcinkowski & Zwell, 1963; Hashimoto & Ogawa, 1970) as well as on the X-ray rotation photograph (Moss, 1966). Characteristic splitting of diffuse scattering in Au–Pd alloys has been observed by Lin, Spruiell & Williams (1970) and Ohshima & Watanabe (1976). Therefore, if the relation between the diffuse scattering and the form of the Fermi surface is to be discussed in terms of the pair-interaction potentials, a sufficient number of potentials must be determined for these alloys too. It seems that the method of analysis using the real-space formalism is not suitable for this purpose, because a large number of potential values must be fitted to a large number of α_{lmn} parameters and an enormous amount of calculation will be necessary. On the other hand, the method using the reciprocal-space formalism, which has been adopted in the present study, is more suitable because a sufficient number of interaction potentials are determined directly from the intensity data by Fourier inversion, though care must be given to the correction of diffuse intensity near the fundamental reflexions.

The authors wish to thank to Professor M. Takahashi of the Department of Applied Physics, Tohoku University, for preparing the single-crystal specimen and Dr M. Tanaka of the Department of Physics for helpful discussion. They also wish to express their appreciation to the Nagoya University Computation Center and the Ministry of Education for support of this work.

References

BLANDIN, A. & DEPLANTÉ, J. L. (1963). *Metallic Solid Solutions*, edited by J. FRIEDEL & A. GUINIER, ch. IV, pp. 1–10. New York: Benjamin.

BORIE, B. & SPARKS, C. J. (1971). *Acta Cryst.* A**27**, 198–201.

CLAPP, P. C. & MOSS, S. C. (1966). *Phys. Rev.* **142**, 418–427.

COWLEY, J. M. (1950). *Phys. Rev.* **77**, 669–675.

ERICSSON, T. & COHEN, J. B. (1971). *Acta Cryst.* A**27**, 97–109.

GRAGG, J. E. JR & COHEN, J. B. (1971). *Acta Met.* **19**, 507–519.

HARRISON, R. J. & PASKIN, A. (1963). *Metallic Solid Solutions*, edited by J. FRIEDEL & A. GUINIER, ch. V, pp. 1–5. New York: Benjamin.

HASEGAWA, K., SUZUKI, T. & HIRABAYASHI, M. (1975). Private communication.

HASHIMOTO, S. & OGAWA, S. (1970). *J. Phys. Soc. Japan*, **29**, 710–721.

HIRABAYASHI, M. & OGAWA, S. (1957). *J. Phys. Soc. Japan*, **12**, 259–271.

KRIVOGLAZ, M. A. (1969). *Theory of X-ray and Thermal Neutron Scattering by Real Crystals.* New York: Plenum Press.

LIN, W. & SPRUIELL, J. E. (1971). *Acta Met.* **19**, 451–461.

LIN, W., SPRUIELL, J. E. & WILLIAMS, R. O. (1970). *J. Appl. Cryst.* **3**, 297–305.
MARCINKOWSKI, M. J. & ZWELL, L. (1963). *Acta Met.* **11**, 373–390.
MOSS, S. C. (1966). *Local Atomic Arrangements Studied by X-ray Diffraction*, edited by J. B. COHEN & J. E. HILLIARD, pp. 95–122. New York: Gordon and Breach.
MOSS, S. C. (1969). *Phys. Rev. Lett.* **22**, 1108–1111.
OHSHIMA, K. & WATANABE, D. (1973). *Acta Cryst.* A**29**, 520–526.
OHSHIMA, K. & WATANABE, D. (1976). *J. Phys. Soc. Japan.* To be published.
PEARSON, W. B. (1958). *A Handbook of Lattice Spacings and Structures of Metals and Alloys.* Oxford: Pergamon Press.
RAETHER, H. (1952). *Angew. Phys.* **4**, 53–59.
ROTH, L. M., ZEIGER, H. J. & KAPLAN, T. A. (1966). *Phys. Rev.* **149**, 519–525.
SATO, K., WATANABE, D. & OGAWA, S. (1962). *J. Phys. Soc. Japan*, **17**, 1647–1651.
SCATTERGOOD, R. O., MOSS, S. C. & BEVER, M. B. (1970). *Acta Met.* **18**, 1087–1098.
SCHUBERT, K., KIEFER, B., WILKENS, M. & HAUFLER, R. (1955). *Z. Metallk.* **46**, 692–715.
SPARKS, C. J. & BORIE, B. (1966). *Local Atomic Arrangements Studied by X-ray Diffraction*, edited by J. B. COHEN & J. E. HILLIARD, pp. 5–50. New York: Gordon and Breach.
STRONG, S. L. & KAPLOW, R. (1967). *Acta Cryst.* **23**, 38–44.
WARREN, B. E. & MOZZI, R. L. (1966). *Acta Cryst.* **21**, 459–461.
WATANABE, D. & FISHER, P. M. J. (1965). *J. Phys. Soc. Japan*, **20**, 2170–2179.
WATANABE, D. & OGAWA, S. (1956). *J. Phys. Soc. Japan*, **11**, 226–239.
WILKINS, S. W. (1970). *Phys. Rev.* (*B*), **2**, 3935–3942.
WILKINS, S. W. & SHIRLEY, C. G. (1975). *J. Appl. Cryst.* **8**, 107–111.
WOOSTER, W. A. (1962). *Diffuse X-ray Reflections from Crystals.* pp. 44–46. Oxford: Clarendon Press.

Acta Cryst. (1976). A**32**, 892

Electrogyration Effect in Alums

BY HANS-J. WEBER AND S. HAUSSÜHL

Institut für Kristallographie der Universität zu Köln, Germany (BRD)

(*Received* 31 *March* 1976; *accepted* 9 *April* 1976)

The electrogyration effect in 31 alums has been measured within the range 350 to 700 nm. The coefficients of electrogyration show an unexpectedly wide variation in alums of different composition and structural type. The effect is obviously related to the symmetry of the constituents and to their bonding interaction with water molecules. The dispersion of the electrogyration can be described by a formula which is also valid for natural optical activity. In contrast to other electro-optical effects Miller's rule does not apply for the electrogyration of the alums.

Introduction

In an earlier paper we reported on electric field induced optical activity (electrogyration) and circular dichroism in chromium-doped $KAl(SO_4)_2 . 12H_2O$ crystals (Weber & Haussühl, 1974). In continuation of that investigation we now have studied the electrogyration in 30 other pure alums in order to obtain an insight into the general behaviour of the effect within a large number of chemically and structurally related crystals. It should be mentioned that the effect of electrogyration only occurs in crystals of symmetry $m3$, without the disturbing influence of birefringence and linear electro-optical effects.

In this point symmetry group the alums crystallize in three different types, called α-, β-, and γ-alums. Structurally they all are closely related (Lipson, 1935). The three modifications possess surprisingly large differences in certain properties, such as morphology, elasticity, thermoelasticity, and thermal expansion (Haussühl, 1961). We expected different behaviour of these three types with respect to the electrogyration effect too.

Measurements

The electrogyration in the crystals under investigation consists of a rotation $\Delta\varrho$ of the plane of polarization of the incident, linearly polarized light. It is optimally observable in the directions of electric field **E** and wave vector **k** as noted in Table 1. The corresponding $\Delta\varrho$ is connected with the only independently existing component, named s_{123}, of the axial third rank tensor of the electrogyration, by

$$\Delta\varrho = (\pi l/\lambda n)\Delta g \,. \qquad (1)$$

In this formula λ is the wavelength, l the length of the specimen parallel to the light path, n the index of refraction and Δg the change of the scalar product $g = \mathbf{G} \,.\, \mathbf{s} = g_{ij} s_i s_j$. **G** is the gyration vector with compo-